STUDY OF SCALAR MACRO- AND MICROSTRUCTURES IN A CONFINED JET

Nikolai Kornev, Valery Zhdanov and Egon Hassel
Lehrstuhl für Technische Thermodynamik,
Universität Rostock
A. Einstein Str. 2, 18059 Rostock, Germany
nikolai.kornev@uni-rostock.de, valerii.zhdanov@uni-rostock.de, egon.hassel@uni-rostock.de

ABSTRACT

The flow structures in a confined jet are studied at high Reynolds and Schmidt numbers using Large Eddy Simulations (LES) and Planar Laser Induced Fluorescence (PLIF) methods. Both the flow mode without the recirculation zone (jet mode) and with the massive separation and creation of the recirculation zone (r-mode) are considered. The scalar field in the r-mode experiences long period temporal oscillations which are in nearly opposite temporal phase at symmetrical points with respect to the pipe centerline. Detailed analysis of vorticity and scalar fields shows that the reason for such flow behavior are coherent vortex structures appearing on the boundary between the jet and the coflow. They induce oscillating motions across the pipe and transport the scalar against the main flow direction within the recirculation zone. Despite of the big difference in the flow modes, the fine scale scalar structures investigated using highly resolved PLIF possess similar statistical properties such as the normalized cumulative distributions and probability densities of the dissipation rate. The fine scalar structures are nearly isotropic with the scalar gradient vector having a slight preference to align with the most compressive strain axis. The scalar field exhibits small-scale intermittency which is strongly dependent on the flow mode.

INTRODUCTION

Mixing in coaxial confined jets has been investigated for a long time because of many practical engineering applications in e.g. combustion chambers, injection systems, chemical mixing devices and many others. In this paper the coaxial axisymmetric jet mixer consisting of a nozzle of diameter d positioned along the center line of a pipe of diameter D has been considered (see Fig. 1 from Kornev et al.(2005)). The fast inner jet (water) with the bulk velocity U_d is confined by a slower outer coflow (water) with velocity $U_D \ll U_d$. The most important parameters determining the mixing process are the flow rate ratio $\dot{V}_D/\dot{V}_d$, the diameter ratio D/d and the Reynolds number $Re_d = dU_d/\nu$.

Most publications on confined jets are about configurations in which the inner jet is much slower than the coflow $U_d/U_D \ll 1$ (see, for instance, Rehab et al. (1997), Mortensen et al. (2003), and Lima and Palma (2002)). These investigations are motivated by two important applications: stabilization of flame fronts by swirl burners and the saturation of air co-flow with molecules of substances transferred by the internal jet. Rehab et al. (1997) revealed and investigated sustaining low-frequency pulsations caused by the recirculating flow cavity arising on the axis in the inner jet region. The structure of this reverse flow zone is similar to the well known wake-type structure behind bluff bodies. Similar phenomena are discussed in this paper for the case of confined coaxial jets with $U_d/U_D \gg 1$ in which the reverse flow region is not on-axis but near the wall.

Surprisingly, the case $U_d/U_D \gg 1$ has attracted less attention although this flow mode is very important for homogenization devices and free jet reactors. Two different flow modes can be observed in jet mixers, depending on the flow rate ratio $\dot{V}_D/\dot{V}_d$ (see Barchilon and Curtet (1964)). If $D/d < \beta(1 + \dot{V}_D/\dot{V}_d)$, where $\beta \approx 1$ is found from a simple entrainment model), the flow is similar to a free jet (henceforth referred to as jet-mode or j-mode for short). If $D/d > \beta(1 + \dot{V}_D/\dot{V}_d)$ a strong flow separation at the pipe walls results in a recirculation zone (see Fig.7 in Zhdanov(2006a)) behind the nozzle (henceforth referred to as recirculation-mode or r-mode for short). A qualitative description of the r-mode is given by Barchilon and Curtet (1964).

The flow phenomena in a jet mixer has been the subject of our previous experimental and numerical works (see Kornev et al. (2005), Zhdanov et al.(2006a), Hassel et al.(2006), Tkatchenko et al.(2007)). Our study showed that the flow in the r-mode is highly unsteady and time averaged results do not describe properly the true nature of flow phenomena typical for this mode. The presence of long period temporal oscillations with a sort of opposition-of-phase of the flow is revealed and quantified.

The present paper focuses on the study of macro- and microstructures in the jet mixer at $U_d/U_D \gg 1$. The following questions are considered:

- What kind of flow structures are responsible for the appearance of sustaining low-frequency oscillations in the r-mode? Why are the oscillations nearly antisymmetric?
- What kind of scalar microstructures are created in a confined jet?
- What are the statistical properties of the microstructures in different flow modes?
- How does the intermittency of the scalar field behave along the jet for different flow modes?
- What is the preferential orientation of the scalar microstructures?
- Which scales do make the main contribution to the scalar variance?

EXPERIMENTAL SETUP

Experiments were made in a closed water pipe for fully developed turbulent liquid flow ($Sc \sim 10^3$) at $Re_d = dU_d/\nu = 10^4$. The diameter ratio was $D/d = 5$. The parameters of experiments are given in table 1. Further details on the experimental setup can be found in Zhdanov et al. (2006a and 2006b). Two different PLIF measurement series have been performed (see table 2). The purpose of the first series with the spatial resolution $300\mu m$ is the investigation of macrostructures of the scalar field whereas the second one with the resolution $31\mu m$ focuses on the study of scalar microstructures. Time resolution in both series is limited by the frequency of laser pulsations of 10 Hz. Mixture frac-

Table 1: Parameters of experiments.

Param.	U_d (ms^{-1})	U_D (ms^{-1})	$\dot{V}_d/\dot{V}_D$
j-mode	1.19	0.06	5.0
r-mode	1.75	0.1	1.3

Table 2: Parameters of PLIF measurements. Ba_9 is the Batchelor scale at $x/D = 9$, t is the laser sheet thickness within the measurement window

Series	Resolution R (μm)	Window (mm)	t (μm)	R/Ba_9
1	300	50×50	300	~ 30
2	31	2.74×2.08	40	~ 3

tion distributions at different x/D are calculated from the emitted rhodamine intensity distributions I referred to the maximum intensity I_0 determined on the centerline in the first cross section at $x/D = 0.1$. The measurements were performed at $0.1 < x/D < 9.0$.

According to our numerical estimations of the dissipation rate the Kolmogorov scale lies in the range between 30μ and 300μ what corresponds to the range of the Batchelor scales between 1μ and 10μ. Therefore, the smallest scalar structures were not resolved in PLIF measurements.

NUMERICAL METHOD

The liquids, we use water, are assumed to be incompressible and miscible. The governing equations are obtained by LES filtering the Navier-Stokes equation, the continuity equation and the transport equation for the mixture fraction f (see Tkatchenko et al.(2007)). The unclosed subgrid stress (SGS) tensor and the subgrid contribution to the scalar dynamics are modeled in terms of filtered quantities using the dynamic mixed model (see, for instance, Sagaut (2003)). The LES code for the numerical solution of governing equations uses an explicit time integration method of 3^{rd} order Runge-Kutta scheme with adaptive time step control at a constant Courant-Friedrich-Lewy (CFL) criterion $CFL = 0.35$. For spatial discretization and for interpolation on a staggered grid arrangement central differences up to 4^{th} order type are used. For the convection terms of the scalar transport equation a total variation diminishing scheme is applied to avoid oscillations due to strong gradient of scalar in the initial part of the nozzle jet. The wall model of Grötzbach and Piomelli (see Sagaut (2003)) was used to avoid high resolution necessary for LES simulations in the wall region. Statistics is calculated using 66 throughflow times based on the bulk velocity of the jet U_d. Numerical calculations are carried out in the computational domain with a length of eight pipe diameters using an inhouse code for LES. In terms of D the computational domain has the size $8 \times 2\pi \times 0.5$ in a cylindrical coordinate system (x, θ, r). A total number of grid cells was varying between $5 \cdot 10^5$ and $2.2 \cdot 10^7$. A thorough validation of the used mathematical model for the jet mixer is given in Tkatchenko et al.(2007). LES has been used for investigations of the flow macrostructures only. Nowadays, the resolution necessary to simulate the scalar microstructures at high Re and Sc numbers considered in this paper is unachievable.

RESULTS

Macrostructures of the flow

Experimental and numerical simulations revealed two remarkable peculiarities of the flow in the r-mode mentioned by Barchilon and Curtet (1964). First, the flow within the recirculation zone is highly unsteady and nearly periodic with a dominating long period mode. The Strouhal number of the dominating mode based on the tube diameter D, the period of oscillations T_c and the incoming co-flow velocity U_D is $Sh = D/U_D T_c \approx 0.12$. Long period oscillations with a dominating frequency are typical for the recirculation area where large vortex clusters are generated. They disappear in areas filled with small scale vortices and scalar structures at $x/D \geq 2$ and in the proximity to the mixer centerline. Dominating oscillations are also not observed in the j-mode. Second, the oscillations at symmetrical points with respect to the centerline ($r/D = 0$) of the jet mixer are nearly antisymmetric. The flow is self-organized in such a way that the most probable event is a mixing increase at one point and a simultaneous mixing decrease at its counterpart with respect to the centerline and vice versa. This interrelation is true in the statistical sense. These facts are clearly supported in the history of the mixture fraction recorded by the PLIF method and the analysis of the autocorrelation function of the mixture fraction fluctuations across the pipe (see Fig. 5 from Hassel(2006)). These two flow phenomena have thoroughly been investigated and documented in our papers (see Zhdanov et al. (2006a) and Hassel et al. (2006)). The aim of the present paper is clarification of the physical mechanisms responsible for the presence of long period antisymmetric oscillations. The PLIF captures only a trace of the scalar field in the measurement plane and don't reflect the three dimensional phenomena. That is why the further analysis is based mostly on LES calculations.

The LES analysis indicates that the reason for the oscillations in the recirculation zone are concentrated vortex structures arising due to instability of primary spanwise vortices. What kind of structures cause the long period antisymmetric oscillations can be understood better by a detailed consideration of the following flow event. Analysis of the mixture fraction field shows that a strong scalar ejection is observed between time instants $t = 27.0$ and $t = 27.027$ seconds at $x/D \approx 1.7$. The two peaks scalar structure designated as SS is shown in Fig. 1. The three dimensional snapshot of the vortex magnitude $|\omega| = [\omega_{\mathbf{x}}^{\mathbf{2}} + \omega_{\theta}^{\mathbf{2}} + \omega_{\mathbf{r}}^{\mathbf{2}}]^{\mathbf{1/2}}$ field (Fig. 2) revealed the presence of two strong vortex structures (VS) located approximately in the same flow area. These can be interpreted as λ-like structures with streamwise legs put into the jet core. The structures are inclined against the main flow direction. The rotational motion inside of the structures is shown in Fig. 2 by curvilinear arrows. The structures induce the motion in the vertical direction which impacts with the pipe wall and leads to the creation of strong secondary vortices on the wall (the area S in Fig. 2). The ascending flow induced by the structures causes the vertical scalar flux shown in Fig. 1.

The interaction between the flow and a vortex structure is schematically illustrated in Fig.3. Through stretching effects the vortex structures can become strong and induce flow and scalar flux towards the pipe wall (Fig.3). It leads to a scalar concentration near the pipe wall above the vortex structures and simultaneously to a deficiency on the opposite side of the pipe cross section. This is the reason for the phase shift of scalar fluctuations at symmetrical points with

respect to the centerline.

Analysis of turbulent fluxes $\overline{u_1' f'}$ and $\overline{u_3' f'}$ supplement the description of the scalar dynamic processes gained from analysis of Fig. 2. Particularly, it was shown that the transfer of the scalar into the recirculation zone occurs mostly by back flow effects (see the flow 1 in Fig.3) rather than by positive transversal transfers of the scalar from the central flow core (see the flow 2 in Fig.3).

When the coflow velocity U_D increases the vortices arising in the primary jet become weaker. They are not able to induce the flow motions across and against the main flow direction which could be strong enough to overcome the coflow. The effects discussed above are weakening and the flow is changing into j-mode.

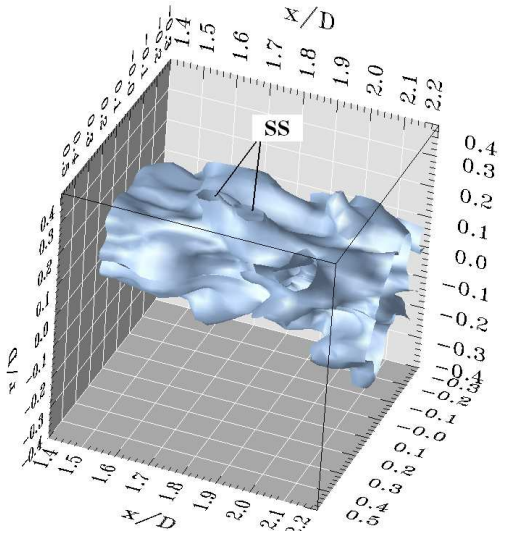

Figure 1: Iso-surface of the mixture fraction $f = 0.425$. SS stands for Scalar Structure under consideration. LES calculation of the r-mode at $t = 27.027$ s.

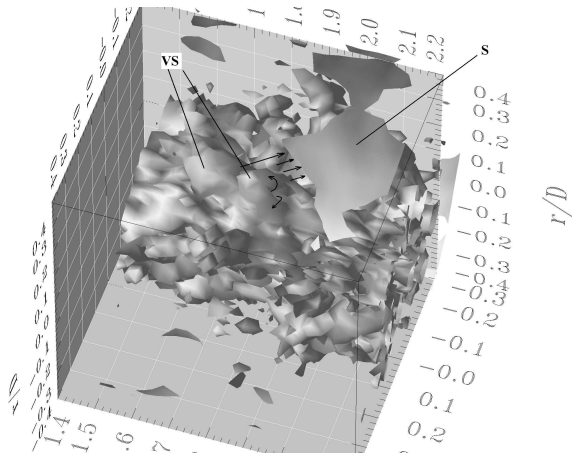

Figure 2: Vortex structures of the flow identified as the iso-surfaces $|\omega| = \mathbf{10^2}$. VS- vortex structures, S- area of the secondary vortices at the pipe wall. LES calculation of the r-mode at $t = 27.027$ s.

Microstructures of the scalar field

The last five problems formulated in the Introduction have been studied using PLIF with the resolution 31 μm. A sample of the spatial spectrum shown in Fig. 4 indicates

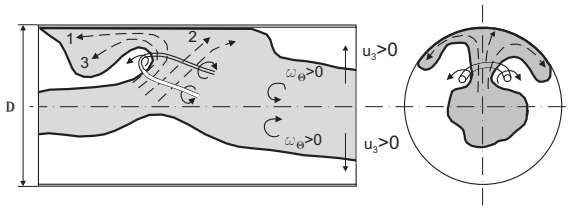

Figure 3: Schematic representation of scalar flux induced by vortex structures.

that the inertial convective range of the spectrum is well resolved for all x/D. A least-squares fit to the Kolmogorov-normalized data gives slopes -1.686 at $x/D = 2$, -1.684 at $x/D = 3$, -1.745 at $x/D = 5$, -1.73 at $x/D = 7$ and -1.68 at $x/D = 9$. At large $x/D = 9$ the resolution 31 μm proved to be enough to resolve the viscous convective range $E_f \sim k^{-1}$ typical for large Schmidt numbers mixing flows.

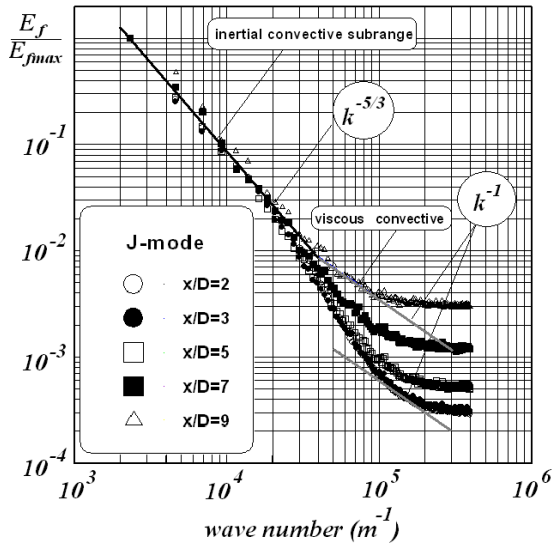

Figure 4: Scalar spectrum at different x/D along the mixer centerline. J-mode.

Structure of the scalar and dissipation rate fields. As mentioned above the large scale scalar structures of the j- and r- modes are quite different. The scalar integral scale is growing up to $x/D \approx 3$ in both flow modes (see Fig.5c in Zhdanov(2006a)). Within the recirculation zone the structures become smaller and the integral scale is decreased at $x/D > 3$. In the j-mode the integral scale is continuing to grow up to $x/D \approx 7$, where the strong interaction between the jet and the pipe wall takes place, and then decreases. This evolution is reflected in sample fields shown in Fig.5 recorded at $x/D = 7$. While scalar layers with thickness of a few dozen microns can be recognized in the j-mode (Fig.5, left), the scalar field in the r-mode (Fig.5, right) seems to be fully smoothed. However, as shown below, the fine scalar structures have certain similar statistical properties in both flow modes. Fig. 6 shows examples of an instantaneous dissipation rate fields $\chi = \nabla f \nabla f(x, y, t)$ obtained from the in-plane projection of the true scalar gradient vector field using the Sobel operator. The dissipation rate maps provide more contrast and allowing the structures to be more readily seen. The scalar dissipation rate is concentrated in thin dissipation layers (see Fig. 6). Three fundamental topologies can be identified in the scalar field. They include

long regions consisting of many straight and nearly parallel dissipation layers, areas where two such long regions meet orthogonally and spiral structures (see Fig. 6).

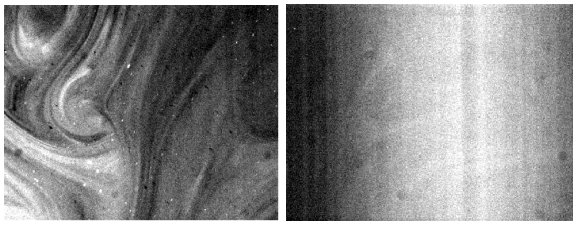

Figure 5: Sample planes at $x/D = 7$ in the j-mode (left) and r-mode (right)

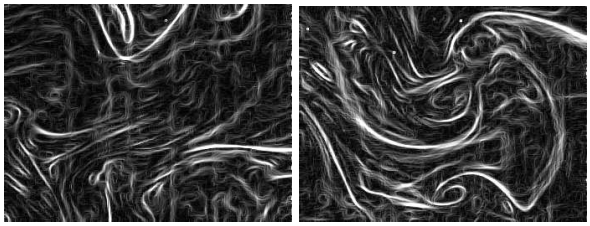

Figure 6: 2D Scalar dissipation rate $\chi = (\frac{\partial f}{\partial x})^2 + (\frac{\partial f}{\partial y})^2$ on the centerline at $x/D = 2$ in the r-mode.

Cumulative distributions and probability densities of the dissipation rate. Fig.7 shows the fraction of the total data volume in which the local scalar dissipation rate is greater than some threshold value χ (see Buch and Dahm(1996)), namely $A_0(\chi) = \int dA_{\chi`>\chi}/dA$, where A is the measurement window area. The rapid drop of A_0, called as the cumulative distribution function(c.d.f), at very low values of χ reflects the fact that the scalar dissipation field is composed primarily of very low values, with high vales occurring infrequently (see Buch and Dahm(1996)). Notice that c.d.f. depends weakly both on the flow mode and on x/D. In accordance with this fact, the p.d.f of the $Log_{10}[\chi/(\overline{f}/D)^2]$ are almost the same for both flow modes (see Fig.8). The curves for $x/D = 7$ were artificially centered on the same mean value of $Log_{10}[\chi/(\overline{f}/D)^2]$. Typical deviations between the experimental data and the Gaussian distribution having the same two first moments are observed. An interesting result of this study is that the similarity laws of the scalar microstructures (e.g. the similarity laws for c.d.f. and p.d.f.) revealed in highly resolved measurements performed by Buch and Dahm(1996) for shear flows hold true in our study although we did not resolve the smallest (Batchelor) scales of the scalar field.

Intermittency. The scalar field is observed to exhibit small-scale intermittency. The scalar difference $\Delta f(r) = f(r) - f(0)$ is non Gaussian and intermittency is observed at inertial range scales (Fig. 9). The intermittency is most pronounced in the front part of the recirculation zone at $x/D = 1$ and $r/D = 0.25$. In the well mixed stage at $x/D > 3$ in the r-mode the scalar difference statistics is almost Gaussian. In the j-mode the intermittency on the centerline is observed up to $x/D = 9$. On the centerline $r/d = 0$ the intermittency is less than at $r/d = 0.25$ for both flow modes. In all measurements the kurtosis tends to the Gaussian value of 3 at large scales and at scales corresponding approximately to the end of the inertial range. Most

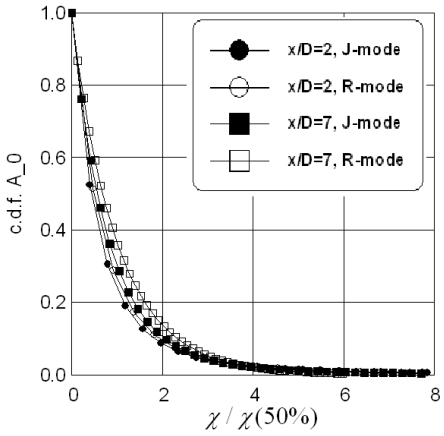

Figure 7: The cumulative distribution function of scalar dissipation rates versus χ normalized with the corresponding measured median dissipation value $\chi_{50\%}$

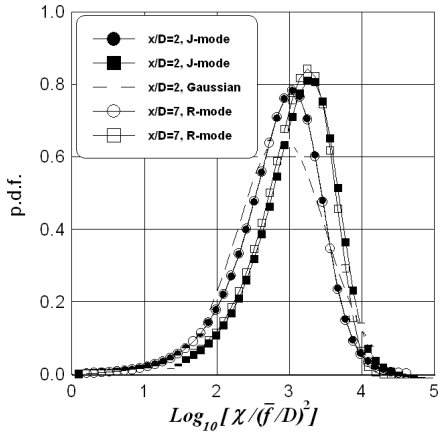

Figure 8: The PDF of the logarithm of the scalar dissipation rate χ.

likely, the latter can be explained by insufficient resolution and noise in the PLIF data.

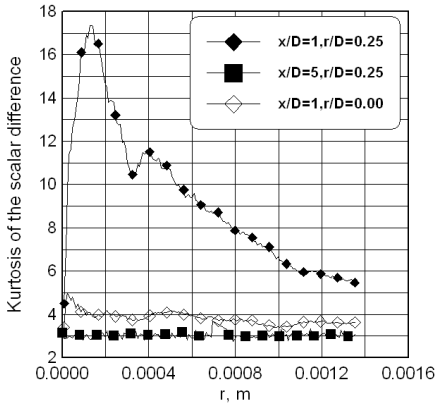

Figure 9: The kurtosis of the scalar difference $\Delta f(r) = f(r) - f(0)$ as a function of the separation r. r-mode.

Small-scale anisotropy and orientation of the scalar structures. Small- scale isotropy is assessed by testing if the measured scalar gradient vector $\nabla f(x, r, t)$ shows any preferred orientation in the p.d.f. distribution of the angle

$\vartheta = tan^{-1}\frac{\partial f/\partial y}{\partial f/\partial x}$ measured in the x,r-plane from the x-axis. The results are shown in Fig. 10 and 11 at different x/D along the mixer centerline both in the r- and the j-modes. If the underlying field $\nabla f(x,r,t)$ were fully isotropic then the distribution of ϑ-values should appear uniform (see Buch and Dahm(1996)). Notice that despite of a quite different structure of the flow in the r- and the j-mode the p.d.f. distributions of ϑ is independent of the flow mode. Since the main flow has its principal compressive strain axis lying along the mixer centerline the p.d.f. distribution has two peaks at $\vartheta = 0$ and $\vartheta = \pm\pi$. At $x/D = 1$ and $x/D > 2$ the most preferred orientation is $\vartheta = \pm\pi$ what is quite expectable since the orientation angle of the mean scalar gradient is $\pm\pi$. However, at $x/D = 2$ the orientations $\vartheta = 0$ and $\vartheta = \pm\pi$ are equally preferred. This is the flow zone where the compressive effects causing the equivalence of the directions $\vartheta = 0$ and $\vartheta = \pm\pi$ are large whereas the mean scalar gradient responsible for the preference of the direction $\vartheta = \pm\pi$ is sufficiently weakened in comparison with that in the section $x/D = 1$ (see Fig. 5a and 5b in Zhdanov et al.(2006a)). At $x/D > 2$ the scalar gradient field is very nearly isotropic with a slight preference of the gradient vector to align with the most compressive strain axis and the mean scalar gradient. Fig. 11 shows the gradient vector orientation angles at $r/D = 0.25$ in the r-mode. The most pronounced anisotropy is detected in the front part of the recirculation zone at $x/D = 1$ whereas at $x/D > 2$ the scalar field is nearly isotropic. The distributions were calculated for all possible scalar gradients vectors (p.d.f (ϑ)), for all vectors corresponding to the dissipation rates larger than the mean dissipation rate χ_m (p.d.f ($\vartheta|\chi > \chi_m$)) and for the vectors corresponding to the dissipation rates larger than $1.2\chi_m$ (p.d.f ($\vartheta|\chi > 1.2\chi_m$)). Such analysis is necessary from two reasons. First, the layers which are orthogonal to the measurement plane are separated from the layers which are oriented at an oblique angle to the laser sheet. Indeed, the thin high-dissipation layers are oriented approximately normal to the measurement plane because a layer that was oriented at an oblique angle with respect to the laser sheet would appear thicker and exhibit lower dissipation. In so doing the disadvantages of the PLIF measurement providing only 2D information can be mitigated. Second, the small structures with high dissipations are separated from large ones which are always present in the recirculation zone. The results show clearly that at $x/D = 1$ the gradient vector of scalar structures corresponding to different dissipation rates has the preferential direction at approximately $\vartheta \approx -50$ deg what is in agreement with the orientation of the most compressive strain axis $\vartheta_{sa} \approx -46$ deg gained from our LES. The orientation of the mean scalar gradient $\vartheta_m = tan^{-1}\frac{\partial\overline{f}/\partial y}{\partial\overline{f}/\partial x} \approx -75$ deg differs from ϑ. Like in the case $r/D = 0$, the scalar gradient field at $r/D = 0.25$ becomes isotropic at large x/D. However, there exists a preferential orientation of the scalar gradient vector which agrees well with the orientation of the most compressive strain axis ($\vartheta_{sa} \approx -42$ at $x/D = 3$ and $\vartheta_{sa} \approx 21$ at $x/D = 5$). No correlation is found between ϑ and ϑ_m.

Contribution of different scales to the scalar variance. The variance of the mixture fraction in liquid mixtures should be larger than in gas mixtures since the diffusion effects characterized by the Schmidt number are sufficiently less in liquids than in gases. This fact which is beyond doubts is explicitly used in the multiple- time- scale (MTS) turbulent mixer

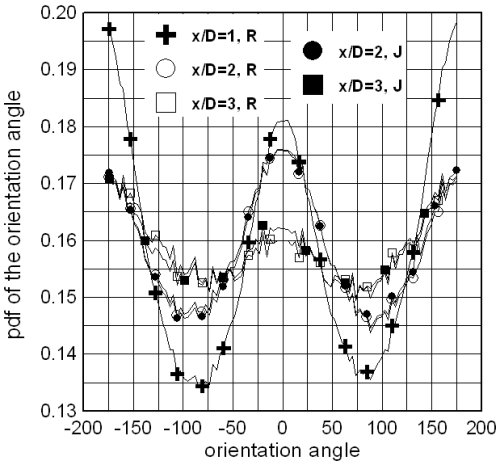

Figure 10: The distribution of the scalar gradient orientation angles at different x/D. $r/D = 0$

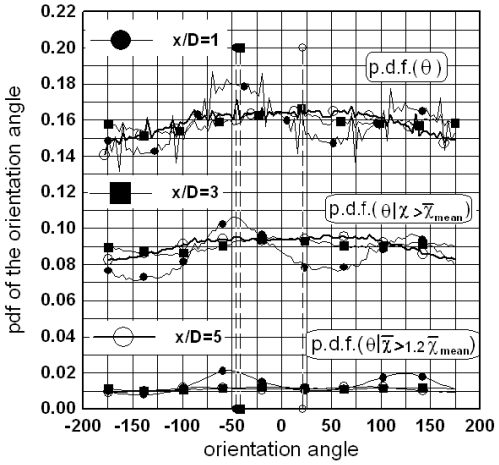

Figure 11: The distribution of the scalar gradient orientation angles at $r/D = 0.25$, r-mode. The vertical dot lines show the orientation of the most compressive strain axis.

model proposed by Baldyga (1999). The local variance σ is represented as the sum of three terms σ_1, σ_2 and σ_3 corresponding to the inertial-convective (σ_1), viscous-convective (σ_2) and viscous- diffusive (σ_3) ranges of the scalar spectrum $E_f(k)$. Results calculated using the MTS model (see Chorny(2007)) are presented in Fig. 12. The PLIF data gained from the first series with the resolution being at $x/D = 9$ thirty times larger than the Batchelor scale agree relatively well with the LES results obtained using the SGS models developed for gas mixtures ($Sc \sim 1$). At first glance the large discrepancy between LES, PLIF and MTS model can be explained by the insufficient resolution of LIF measurements and by gaps in SGS modeling. One could expect that the tenfold increasing the resolution in the second LIF series should result in a sufficient increase of the mixture fraction variance and in the reduction of the discrepancy between MTS and LIF data. However, new LIF data are proved to be very close to the old ones and they agree almost perfectly with the LES. The further analysis showed that the dominating contribution to the scalar variance is made by large scale oscillations corresponding to the energy containing and inertial convective subranges of the spectrum. The contribution from oscillations with scales of a few Batchelor lengths, which were not resolved in the first LIF series and

not taken into account in the SGS LES models, is minor, i.e $\sigma_1 \gg \sigma_2$ and $\sigma_1 \gg \sigma_3$. Obviously, this the reason why the LES models originally developed for the case $Sc \sim 1$ provide quite reasonable results for the scalar variance in liquid mixtures. The discrepancy between the RANS MTS model and measurements can be explained by general disadvantages of the RANS technique compared with LES (see Tkatchenko et al.(2007)) and by sufficient overestimation of σ_2 and σ_3 contributions in the MTS model.

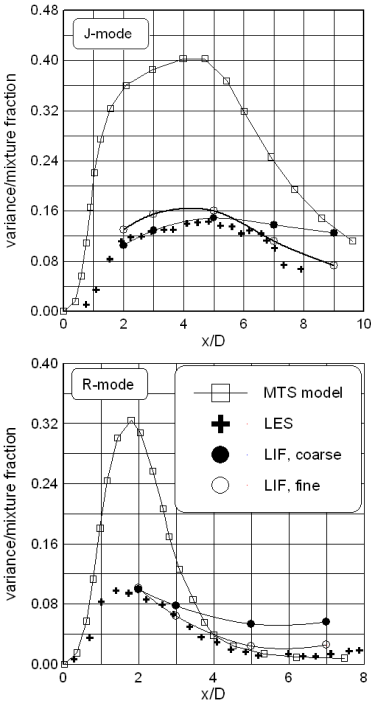

Figure 12: Mixture fraction variance versus x/D for j- and r-modes.

CONCLUSIONS

The macrostructures of the flow in a confined jet configuration depend strongly on the flow mode. In the j-mode the structures are similar to those of the free jet. In the r-mode the coherent vortex structures with dominant streamwise components of vorticity cause oscillations containing a dominating long period mode. These structures arising periodically in the primary nozzle jet cause scalar ejections towards the pipe wall and propagation of the scalar against the main flow. Due to the vortex induced transversal and axial motions the scalar concentration increases on one side of the pipe and decreases on the opposite one. As a result the phase shift of scalar fluctuations is observed at symmetrical points with respect to the pipe centerline. Schematically, a typical scenario which leads to the phase shifted scalar oscillations is shown in Fig.3. These vortex structures become weaker as the coflow velocity U_D increases. The effects discussed above get smaller and the flow is changing into j-mode.

Despite of the big difference in the structure of the macroflow, the fine scale scalar structures possess certain similar statistical properties. For instance, the normalized cumulative distributions and probability densities of the dissipation rate are almost the same for all flow modes. The scalar field is observed to exhibit small-scale intermittency which is strongly dependent on the flow mode. The intermittency is most pronounced in the front of the recirculation zone and becomes weaker on the centerline and downstream. In a well mixed stage the scalar field has Gaussian statistics. The scalar gradient vector is aligned with the orientation of the most compressive strain axis. For the flow under consideration the most contribution to the scalar variance is made by large scale motions.

ACKNOWLEDGMENT

The authors acknowledge gratefully the support of the German Research Foundation (DFG) through the program SPP 1141.

REFERENCES

Kornev, N., Tkatchenko, I., Zhdanov, V., Hassel, E., and Jahnke, S., 2005, "Simulation and measurement of flow phenomena in a coaxial jet mixer," *Proceedings, 4th International Symposium Turbulence and Shear Flow Phenomena*, J.A.C. Humphrey et al., ed., Williamsburg, VA USA, Vol. 2, pp. 723-728.

Rehab, B., Villermaux, E., and Hopfinger, E., 1997, "Flow regimes of large-velocity-ratio coaxial jet", *J. Fluid Mech.*, Vol.345, pp. 357-381.

Mortensen, M., Orciuch, W., Bouaifi, M., and Andersson, B., 2003, "Mixing of a jet in a pipe", *Trans IChemE*, Vol. 81 A, pp. 1–7.

Lima, M., and Palma, J., 2002, "Mixing in coaxial confined jets of large velocity ratio", *Proceedings, 10th Intern. Symp. on Application of Laser Technique in Fluid Mechanics,* Lisboa, 8-11 July.

Barchilon, M., and Curtet, R., 1964, "Some details of the structure of an axisymmetric confined jet with backflow ", *J. Basic Engineering*, pp. 777-787.

Zhdanov, V., Kornev, N., Hassel, E., and Chorny, A., 2006a, "Mixing of confined coaxial flows", *Intl. Journal of Heat and Mass Transfer*, Vol. 49, pp. 3942-3956.

Hassel, E., Jahnke, S., Kornev, N., Tkatchenko, I. and Zhdanov, V., 2006, "Large-Eddy Simulation and laser diagnostic measurements of mixing in a coaxial jet mixer",*Chemical Engineering Science*, Vol. 61, pp. 2908-2912.

Tkatchenko, I., Kornev, N., Jahnke, S., Steffen, G. and Hassel, E., 2007, "Performances of LES and RANS models for simulation of complex flows in a coaxial jet mixer", *Flow, Turbulence and Combustion*, Vol. 78, pp. 111-127.

Zhdanov, V., Kornev, N., and Hassel, E., 2006b, "LIF identification of the microstructures in an axial jet mixer", *Proceedings, 14th Conference GALA*, Braunschweig, Germany, pp. 32.1-32.8

Sagaut, P., 2003,. "Large Eddy Simulations for Turbulent Incompressible Flows", Springer.

Buch, K.A., and Dahm, W.J.A., 1996, "Experimental study of the fine-scale structure of conserved scalar mixing in turbulent shear flows ", *J. Fluid Mech.*, Vol. 317, pp. 21-71.

Baldyga, J., and Bourne, J.R., 1999, "Turbulent Mixing and Chemical Reactions", John Wiley and Sons.

Chorny, A.D., Kornev, N.V., and Hassel, E., 2007, "Simulation of the passive scalar mixing in the jet mixer", submitted to the Russian Journal of Thermophysics.